Supporting Information

Quevillon-Cheruel et al. 10.1073/pnas.1205638109

SI Materials and Methods

Expression and Purification of DprA from *Escherichia coli*. The *Escherichia coli* BL21-Gold(DE3) strain (Stratagen) was transformed with pKHS-*dprA* and grown at 37 °C in 2× YT medium (BIO 101, Inc.). At an OD_{600} of ∼1, protein expression was induced with 0.5 mM isopropyl β-D-1-thiogalactopyranoside (Sigma), and cells were grown for a further 4 h. Cells were harvested by centrifugation, resuspended in 40 mL of buffer L [50 mM MES (pH 6.5) and 2 M NaCl] and stored at −20 °C. Cell lysis was completed by sonication (with a Branson probe-tip sonicator). Soluble His-tagged DprA was retained on a Ni-NTA column (Qiagen Inc.), eluted with the same buffer complemented with imidazole (200 mM), concentrated on a Vivaspin 5000 centrifugal concentrator (Vivascience), and loaded onto a SuperdexTM200 column (Amersham Pharmacia Biotech) equilibrated against 50 mM MES (pH 6.5), 2 M NaCl. Selenomethionine-labeled protein was prepared as described (1) and purified as the native protein. The various DprA mutants were expressed and purified in the same manner.

Crystallization, Data Collection, Structure Determination, Model Building, and Refinement. Crystallization trials of selenium-labeled DprA were performed using the sitting drop vapor-diffusion method at 18 °C using a 100-nL drop-dispensing robot (Cartesian), with protein concentrations varying from 3–8 $mg{\cdot}mL^{-1}$. A sparse-matrix screen allowed initial crystallization conditions to be obtained [Nextal Procomplex Suite from QIAGEN, condition 86: 0.1 M MES (pH 6.5), 1 M $LiSO_4$]. Refinement of the conditions was performed by hand. Crystals appeared within 3–10 d. They were treated briefly with a cryoprotectant identical to the mother liquor, except that 25% of the water was replaced by sorbitol. This treatment allowed them to be flash frozen at 100 K before exposure to X-rays. Data were collected at 0.9796 Å using the oscillation method on the Proxima-1 beamline at the SOLEIL synchrotron facility (Saclay, France), which is equipped with a Q315r detector (ADSC). One dataset of 90° was collected with 0.25° oscillation frames. Data processing was done with XDS and XSCALE (2), as well as with the CCP4 suite of programs (3). The crystals belong to the tetragonal space group $I4_122$, with unit cell parameters $a = b = 297.64$ Å, $c = 82.01$ Å and $a = b = 300.24$ Å, $c = 78.33$ Å, respectively, for two individual selenium-labeled crystals. Statistics from the data collection are summarized in Table S1. The first crystal was used for a single-wavelength anomalous dispersion (SAD) experiment. After processing, SHELX (4) was used to attempt to locate 15 heavy atom sites, using reflections from 20- to 3.4-Å resolution. After solvent flattening and phase improvement of the resulting electron density map using density modification as implemented in RESOLVE (5), an initial partial model was built automatically. A second complete data set then was collected at the European Synchrotron Research Facility (Grenoble, France) using another crystal and helped obtain a complete model at 2.7-Å resolution. Initial refinement of the atomic model of DprA was performed using PHENIX.REFINE for simulated annealing using a phased maximum-likelihood target function (6). Later rounds of refinement were performed with REFMAC with maximum likelihood analysis and including the phase information from the SAD experiment (7, 8), with intermittent rounds of model building with COOT (9) and O (10). During initial rounds of refinement, phase restraints and noncrystallographic symmetry restraints were included. Validation of the structure was performed using MOLPROBITY (11). Statistics of the refined model of DprA are summarized in Table S1.

3D Structure Comparison and 3D Model Building. The Dali server was used to compare 3D protein structures (12). 3D protein comparative modeling was performed using a SWISS-MODEL server (13). We used the 3D coordinates of $_{Sp}$DprA (this study) to construct models for $_{Rp}$DprA and $_{Ec}$DprA (QMEAN Z-score = −2.912 and −3.627, respectively) (Fig. S6*E*) and used $_{Rp}$DprA coordinates to construct models for $_{Sp}$DprA (QMEAN Z-score = −4.429) (Fig. S6*D*), with SWISS-MODEL. The PyMOL Molecular Graphics System (version 1.3; Schrödinger, LLC.) was used to create structure views.

Exploration of $_{Sp}$DprA and $_{Rp}$DprA Dimerization Interface. Exploration of C/C DprA interfaces (Table S2) was performed using PDBePISA tool (14). The percent accessibility of residue X in the monomer corresponds to the accessible surface area (ASA) value for X divided by the total accessible surface area of the amino acid side chain for X in a Gly-X-Gly tripeptide with the main chain in an extended conformation (15, 16). The percent accessibility in the dimer was calculated by dividing the percent accessibility of residue X in the monomer by the buried area percentage (i.e., the surface of residue X involved in C/C dimer interface) for the same residue generated by PDBePISA.

Small-Angle X-Ray Scattering Data Acquisition and Processing and Model Construction. Small-angle X-ray scattering (SAXS) data were averaged and background subtracted using the program package PRIMUS (17). Intensities were put on an absolute scale using water scattering. Measurements were performed at 15 °C in a buffer composed of 20 mM Tris·HCl (pH 7.5), 1 M NaCl, 5% (vol/vol) glycerol for DprA (on Nanostar, Bruker) and 20 mM Tris·HCl (pH 7.5), 2 M NaCl, 5% (vol/vol) glycerol for $DprA^{AR}$ or $DprA^{VR}$ (on SWING, at the synchrotron SOLEIL). For comparison, the curves were normalized to protein concentration and to a term accounting for contrast: $K = \left(\frac{mN_a}{M} - \bar{v}_p\rho_s\right)^2$ where m is the number of electrons, M the molar mass, N_a the Avogadro number, $\bar{v}_p$ the partial specific volume, and ρ_s the solvent electron density. Extrapolated forward scattering $I(0)$ was determined by Guinier approximation from the low q-region of the scattering profiles, also yielding the value of the radius of gyration (Rg): $\ln I(q) = \ln I(0) - Rg2q2/3$. The molar mass of the scattering objects and consequently the oligomerization state of the proteins were derived from the value of $I(0)$. For DprA, because of a slight effect of the protein concentration, the curve shown in Fig. 3*A* was obtained by splicing the data measured at 1.6 $mg{\cdot}mL^{-1}$ (for the high q-range) and 0.8 $mg{\cdot}mL^{-1}$ (for the low q-range). For $DprA^{AR}$, no effect caused by the concentration was observed; the curve shown in Fig. 3*B* was measured at a concentration of 2.1 $mg{\cdot}mL^{-1}$.

The molar mass also was obtained independently from the whole $I(q)$ curve using the Porod volume and the program Autoporod developed by Svergun's team (ATSAS package at http://www.embl-hamburg.de/biosaxs/software.html) or the method elaborated by Craievich's team (18).

Scattering patterns from crystal structures were calculated using the program CRYSOL (19) and then were adjusted to the experimental curve. During this procedure the His-tag, absent in the crystal structure, was added. The quality of the fits was characterized by the χ parameter:

$$\chi^2 = \frac{1}{N-1}\sum_j \left[\frac{I_{\exp}(q_j) - cI_{calc}(q_j)}{\sigma(q_j)}\right]^2$$

where N is the number of experimental points, c is a scaling factor, and $I_{calc}(q_j)$ and $\sigma(q_j)$ are the calculated intensity and the experimental error at the scattering vector q_j.

Finally we determined the envelope of the scattering object (dimer and monomer) using the ab initio program GASBOR (20), which describes it as a chain of dummy residues (Fig. 3 *C* and *D* and Fig. S3*C*). After this calculation was repeated 20 times, the program DAMAVER (21) was used to align the different shapes and to select the most typical reconstruction. The crystal structure then was superimposed over the most representative ab initio model using the program SUBCOMB (22). The quality of the superimposition was quantified using the normalized spatial discrepancy (NSD) parameter (22). The smaller this value, the more similar are the two compared models. When comparing an ab initio model and an atomic structure, values close to 1 suggest a very good agreement.

SAXS Data Analysis. First, DprA *M* derived from the intensity at the origin *I(0)* was of the order of 60 kDa with an error smaller than 10%. The value obtained using the Porod volume was in the same range, 65 ± 5 kDa.

Second, the shape of the scattering object (i.e., DprA) was reconstructed from the experimental curve with GASBOR. The superimposition of the tail-to-tail (C/C) crystallographic dimer on the reconstructed volume (Fig. 3*C*) was quite satisfactory, with an NSD factor of 1.19. Nevertheless, the envelope obtained from SAXS data appeared somewhat more closed than the crystal structure. Thus, a slight flexibility between the two monomers with a deviation angle of 20–30° compared with the dimer in the crystal, as well as some flexibility within the linker between sterile alpha motif (SAM) and Rossmann fold-like domains, cannot be excluded. The existence of a deviation also was suggested when adjusting the calculated curve from the C/C crystal structure to the experimental one using Crysol. The adjustment was good (χ = 1.2) but not perfect, as revealed by the behavior of the residuals (Iexp(q)-Icalc(q) (Fig. S3*D*). The comparison of the distance distributions functions P(r), calculated and experimental, also led to the same conclusion (Fig. S3*E*).

Third, a similar analysis performed using the SAM/SAM (N/N) dimer indicated a slightly weaker fit between the calculation from the N/N dimer and the experimental data (Fig. S3 *B*–*E*). The adjustment of the calculated curve *I(q)* and the superimposition of the N/N crystallographic dimer on the envelope gave χ = 1.8 and NSD = 1.42, respectively. The calculated curve P(r) also differed significantly from the experimental curve. Together, these results established unambiguously that purified DprA self-assembles as a dimer in solution, more likely a C/C than N/N dimer.

Random Mutagenesis and Selection for DprA Interaction Mutants Using a Yeast Two-Hybrid Assay. Mutational mapping of the DprA interaction surface with RecA was performed using a recently developed strategy based on a GAL4-derived yeast two-hybrid (Y2H) assay (23). The *dprA* coding sequence was subjected to random mutagenesis by error-prone PCR favoring single mutational events as described (23). The library of the mutated *dprA* gene-coding sequence, fused with the functional binding domains (BD) of GAL4, was established in the yeast PJ69-4 (α) haploid strain using the gap-repair procedure and arrayed in the 96-well plate format. An array of 1,500 colonies per library, expressing potential DprA mutant proteins, was mated with PJ69-4 (α) strains expressing either RecA or DprA proteins in fusion with the complementary GAL4 functional domain. Diploids were monitored for the expression phenotypes, i.e., for their ability to grow on selective media lacking uracil, leucine, histidine, or adenine (−LUH and −LUA). Diploid colonies that specifically failed to grow on selective media were screened. A particular focus was given to diploids that specifically failed to express the interaction phenotypes when DprA was coexpressed with RecA but retained the ability to self-interact. The corresponding haploid clones harboring the DprA mutant derivatives (from the library) were pooled and tested again for the loss of interaction phenotypes. The corresponding mutations within *dprA* were identified by sequencing.

Site-Targeted Mutagenesis and Analysis of Interaction Phenotypes in Y2H. Site-directed saturation mutagenesis of *dprA* was performed by PCR amplification and fragment joining using degenerated oligonucleotides containing a randomized codon at the targeted position. The mutated PCR-amplified *dprA* coding sequences were digested and inserted in frame with the BD domain of Gal4 into the pGBDU vector by ligation and transformation of *E. coli*. Mutant derivatives of *dprA* were PCR-amplified from individual colonies, and single mutations were identified by sequencing. The pGBDU-*dprA* constructs carrying a point mutation then were transferred into the pJ69-4 (a) yeast haploid strain.

Yeast haploid cells containing the pGBDU-*DprA* mutant derivatives were mated with haploid strains of opposite mating type harboring the pGAD-partner constructs that expressed RecA or DprA itself. Interacting phenotypes were assessed according to the ability of the diploid forms to grow on selective media depleted of histidine (−LUH) or adenine (−LUA) or on −LUH media supplemented with 10 mM 3-aminotriazol.

Pneumococcal Transformation. Pneumococcal stock cultures were grown at 37 °C in Todd–Hewitt (BD Diagnostic System) plus yeast extract medium to an OD_{550} of 0.3 and were stored at −80 °C after the addition of 15% glycerol. Transformation experiments were performed in C+Y medium by treating precompetent cells at 37 °C for 10 min with synthetic competence-stimulating peptide CSP1 (100 ng·mL^{-1}), as previously described (24). Upon addition of chromosomal DNA (unless otherwise indicated), cells were incubated for 20 min at 30 °C. Transformants were plated on CAT-agar supplemented with 4% horse blood and, after phenotypic expression for 120 min at 37 °C, were selected by using a 10-mL CAT-agar overlay containing erythromycin (0.05 μg·mL^{-1}), kanamycin (250 μg·mL^{-1}), or streptomycin (200 μg·mL^{-1}).

Plasmid Constructions. Plasmids pKHS-*dprA* and pKHS-*dprA*$^{I251V\text{-}H260R}$ were constructed into the pKHS vector (25). PCR fragments generated with the primers SC*dprA*-1 (with an EagI site) and SC*dprA*-2 (with a NotI site) (Table S5) on genomic DNA from *Streptococcus pneumoniae* R800 and yeast D10 recombinant plasmid, respectively, were cut by EagI and NotI and were ligated into pKHS linearized by EagI to generate pKHS-*dprA* and pKHS-*dprA*$^{I251V\text{-}H260R}$. pKHS-*dprA*$^{H260A\text{-}L269R}$ was constructed by site-directed mutagenesis using the QuikChange II kit from Stratagene, with pKHS-*dprA* as template and SC*dprA*^{AR}-1 and SC*dprA*^{AR}-2 as primers. Three alanine and six histidine codons provided by the pKHS vector were present in frame at the 3′ end of the genes. pET28-*dprA*$^{E235Q\text{-}D243N\text{-}E265Q}$ was created by cloning the NcoI-XhoI fragment containing the *dprA*$^{E235Q\text{-}D243N\text{-}E265Q}$ sequence from the plasmid pUC57-*dprA*$^{E235Q\text{-}D243N\text{-}E265Q}$ (constructed by GenScript) between the NcoI and XhoI sites of the pET28 vector. In this plasmid, the start codon of *dprA*$^{E235Q\text{-}D243N\text{-}E265Q}$ is part of the NcoI restriction site, resulting in the addition of a glycine after the initiation methionine.

To achieve ectopic expression of *recA* and *dprA* in *S. pneumoniae*, we constructed derivatives of $pCEP_X$, an integrative plasmid that allows chromosomal integration of a gene at CEP

(26) and its expression under the control of the CSP-inducible, ComX-dependent promoter of the *ssbB* gene, P_X (27). pCN9 (i.e., pCEP$_X$-*recA*-SPA) was created in a three-way ligation with (*i*) a NcoI-XhoI PCR product containing the *recA* ORF (generated with the RecA9 and RecA8 oligonucleotides and genomic DNA from strain R304 as template); (*ii*) a XhoI-BamHI PCR product containing the sequential peptide affinity (SPA) tag sequence (28) (generated with the SPAtag1 and SPAtag3 oligonucleotides on pMutin-SPA (29) as template DNA); and (*iii*) pCEP$_X$ cut with NcoI and BamHI. In this plasmid, the start codon of *recA* is part of the NcoI restriction site, resulting in the addition of a glycine after the initiation methionine. To generate plasmid pCN55 (i.e., pCEP$_X$-*dprA*-SPA), a BspHI-XhoI PCR product containing the *dprA* ORF (oligonucleotide oCN26 and DprA23 and genomic DNA from strain R304 as template) and a XhoI-BamHI fragment containing the SPA tag sequence from pCN9 were inserted into pCEP$_X$ cut with NcoI and BamHI. Plasmid pCN58 (i.e., pCEP$_X$-*dprA*^{AR}-SPA) was generated by ligating a BspHI-XhoI PCR product containing the *dprA*$^{H260A\text{-}L269R}$ mutant ORF (oligonucleotide primers oCN26 and DprA23 and template DNA pKHS-*dprA*$^{H260A\text{-}L269R}$), a XhoI-BamHI fragment containing the SPA tag sequence from pCN9, and the pCEP$_X$ vector cut with NcoI and BamHI. Similarly, pCN56 (i.e., pCEP$_X$-*dprA*^{VR}-SPA) was created by ligating a BspHI-XhoI PCR product containing the *dprA*$^{I251V\text{-}H260R}$ mutant ORF (oligonucleotide primers oCN26 and DprA23 and genomic DNA from strain R2187 as template), a XhoI-BamHI fragment containing the SPA tag sequence from pCN9, and the pCEP$_X$ vector cut with NcoI and BamHI.

pCN21 (i.e., pCEP$_X$-*gfp$_{mut2}$*-SPA), an integrative plasmid that allows expression of the *gfp$_{mut2}$* allele (30) fused to the *SPA* tag sequence under the control of the CSP-inducible P_X promoter was constructed in a three-way ligation with (*i*) a BspHI-XhoI PCR product containing the *gfp$_{mut2}$* ORF [generated with the oCN21 and oCN25 oligonucleotides and template DNA pKL147 (31)]; (*ii*) a XhoI-BamHI PCR product containing the SPA tag sequence from pCN9; and (*iii*) pCEP$_X$ cut with NcoI and BamHI.

Constructions of Pneumococcal Mutants Containing *dprA* Mutations. Plasmids containing the *dprA* mutations identified by Y2H were extracted from yeast, propagated into *E. coli* LE392 cells (32), and used to transform *S. pneumoniae* strain R1818. After allowing a few hours for phenotypic expression and cell segregation in liquid culture without selection, aliquots of the transformed culture were plated, and 10 independent colonies were isolated. Presence of the mutations was confirmed by sequencing the entire *dprA* coding sequence.

To construct *dprA*$^{H260A\text{-}L269R}$, *dprA*$^{E235Q\text{-}D243N}$, and *dprA*$^{E235Q\text{-}D243N\text{-}E265Q}$ pneumococcal mutants, plasmid pKHS-*dprA*$^{H260A\text{-}L269R}$ and pET28-*dprA*$^{E235Q\text{-}D243N\text{-}E265Q}$ were used to transform the *S. pneumoniae* strains R1501 or R1818 without selection, as described above. R2585 (*dprA*$^{H260A\text{-}L269R}$), R2830 (*dprA*$^{E235Q\text{-}D243N\text{-}E265Q}$), and R2832 (*dprA*$^{E235Q\text{-}D243N}$) were retained after sequencing the entire *dprA* coding sequence.

Purification of SPA-Tagged Proteins from Pneumococal Cells. The tagged proteins DprA-SPA and RecA-SPA, ectopically expressed from CEP (see above) in *dprA*$^+$, *recA*$^+$ competent cells (Table S4), complemented the transformation defect of *dprA*-null and *recA*-null mutant strains respectively, demonstrating that the DprA-SPA and RecA-SPA fusions are functional (albeit, in the latter case, not fully functional, as revealed by a 5- to 10-fold reduction in transformation frequency compared with wild type). Purifications were performed from 250-mL cultures of strains containing the SPA tag constructs at an OD_{550} of ~0.14 in C+Y medium treated with 25 μg of CSP-1 at 37 °C for 12 min. Harvested cells were washed in buffer A [10 mM Tris·HCl (pH 7.5), 0.15 M NaCl], frozen in liquid nitrogen, and kept at −80 °C until purification. Thawed cell pellets were resuspended in 1,250 μL buffer B [10 mM Tris·HCl (pH 7.5), 0.15 M NaCl, 0.2 mM EDTA, 0.1% (vol/vol) Triton ×100] supplemented with 1 mM PMSF, incubated on ice for 20 min, at 37 °C for 20 min, and refreshed on ice for 10 min. Soluble whole-cell extracts were collected after sonication and centrifugation at 20,000 × *g* for 30 min at 4 °C. All subsequent steps were performed at 4 °C unless otherwise indicated. Cell extracts were incubated with 10 U of benzonase nuclease (Novagen) for 30 min. The benzonase-treated soluble extract (the load, indicated by "L" in the figures) was mixed with 200 μL anti-FLAG M2 agarose beads (Sigma) and rotated for 4 h. Agarose beads were pelleted at 2,700 × *g*, and the supernatant (the flow through, indicated by "FT1" in the figures) was removed. Beads were transferred into Bio-Spin columns (Bio-Rad), washed five times with 400 μL of buffer B, and suspended in 200 μL of TEV buffer [50 mM Tris·HCl (pH 7.5), 0.15 M NaCl, 0.2 mM EDTA, 0.1% Triton X-100, 1 mM DTT]. Fifty units of AcTEV protease (Invitrogen) were added, and beads were incubated 18 h with rotation. Eluted proteins (referred to as "C1" in the figures) were analyzed directly by immunoblot or were subjected to a second-step purification procedure as previously described (29). Specifically, in this second-step purification, eluted proteins were incubated in a new, fresh Bio-Spin column with 400 μL of TEV buffer supplemented with 5 μL of 240 mM $CaCl_2$ and 50 μL of Calmodulin-Sepharose beads (Amersham Biosciences) for 3 h. The flowthrough from the calmodulin Sepharose column (FT2 in Fig. S5*D*) was collected. Beads then were washed with 500 μL of buffer CBB [10 mM Tris·HCl (pH 7.5), 0.15 M NaCl, 2 mM $CaCl_2$, 10 mM β-mercaptoethanol] and 100 μL of buffer CWB [10 mM Tris·HCl (pH 7.5), 0.15 M NaCl, 0.1 mM $CaCl_2$, 10 mM β-mercaptoethanol]. Finally, protein complexes (C2 in Fig. S5*D*) were eluted with 500 μL of CEB buffer [50 mM Tris·HCl (pH 7.5), 0.15 M NaCl, 3 mM EGTA, 10 mM β-mercaptoethanol] and analyzed by immunoblot after trichloroacetic acid/acetone precipitation. Equivalent amounts of the load (L) and flowthrough from the anti-FLAG M2 agarose column (FT1) were analyzed.

As a control for nonspecific retention and release of proteins of interest, purifications were performed from a strain harboring a GFP-SPA fusion (Fig. 3*F*). This heterologous fusion protein was expressed from the Px promoter and therefore was synthesized during competence.

Western Blot Analysis. An equal volume of 2× SDS sample buffer [0.25 M Tris (pH 6.8), 6% (wt/vol) SDS, 10 mM EDTA, 20% (vol/vol) glycerol] containing 10% (vol/vol) β-mercaptoethanol was added to protein samples. Samples were heated for 5 min at 80 °C before loading. Proteins were separated by SDS/PAGE on 12% (wt/vol) polyacrylamide gels, electroblotted onto Protran nitrocellulose membranes (Whatman), and blocked in 8% (wt/vol) skimmed milk in TBS (50 mM Tris·HCl, 150 mM NaCl, pH8) containing 0.1% (vol/vol) Tween 20. The blocked membrane was probed with anti-RecA or anti-DprA antibodies. Primary antibodies were diluted 1:10,000 into 5% (wt/vol) skimmed milk in TBS–0.01% (vol/vol) Tween 20. Primary antibodies were detected using peroxidase-conjugated goat anti-rabbit IgG (Sigma) with the ECL Western Blotting Detection System (GE Healthcare) and a luminescent image analyzer (LAS-4000; Fuji).

1. Quevillon-Cheruel S, et al. (2007) Cloning, production, and purification of proteins for a medium-scale structural genomics project. *Methods Mol Biol* 363:21–37.

2. Diederichs K (2006) Some aspects of quantitative analysis and correction of radiation damage. *Acta Crystallogr D Biol Crystallogr* 62:96–101.

3. Collaborative Computational Project N4 (2004) The CCP4 suite: Programs for protein crystallography. *Bioinformatics* 22:195–201.
4. Sheldrick GM (2010) Experimental phasing with SHELXC/D/E: Combining chain tracing with density modification. *Acta Crystallogr D Biol Crystallogr* 66:479–485.
5. Terwilliger TC (2000) Maximum-likelihood density modification. *Acta Crystallogr D Biol Crystallogr* 56:965–972.
6. Terwilliger TC, et al. (2008) Iterative model building, structure refinement and density modification with the PHENIX AutoBuild wizard. *Acta Crystallogr D Biol Crystallogr* 64:61–69.
7. Murshudov GN, Vagin AA, Dodson EJ (1997) Refinement of macromolecular structures by the maximum-likelihood method. *Acta Crystallogr D Biol Crystallogr* 53: 240–255.
8. Pannu NS, Murshudov GN, Dodson EJ, Read RJ (1998) Incorporation of prior phase information strengthens maximum-likelihood structure refinement. *Acta Crystallogr D Biol Crystallogr* 54:1285–1294.
9. Emsley P, Cowtan K (2004) Coot: Model-building tools for molecular graphics. *Acta Crystallogr D Biol Crystallogr* 60:2126–2132.
10. Jones TA, Zou JY, Cowan SW, Kjeldgaard M (1991) Improved methods for building protein models in electron density maps and the location of errors in these models. *Acta Crystallogr A* 47:110–119.
11. Davis IW, Murray LW, Richardson JS, Richardson DC (2004) MOLPROBITY: Structure validation and all-atom contact analysis for nucleic acids and their complexes. *Nucleic Acids Res* 32(Web Server issue):W615-9.
12. Holm L, Rosenström P (2010) Dali server: Conservation mapping in 3D. *Nucleic Acids Res* 38(Web Server issue):W545-9.
13. Arnold K, Bordoli L, Kopp J, Schwede T (2006) The SWISS-MODEL workspace: A web-based environment for protein structure homology modelling. *Bioinformatics* 22: 195–201.
14. Krissinel E, Henrick K (2007) Inference of macromolecular assemblies from crystalline state. *J Mol Biol* 372:774–797.
15. Miller S, Janin J, Lesk AM, Chothia C (1987) Interior and surface of monomeric proteins. *J Mol Biol* 196:641–656.
16. Miller S, Lesk AM, Janin J, Chothia C (1987) The accessible surface area and stability of oligomeric proteins. *Nature* 328:834–836.
17. Konarev PV, Volkov VV, Sokolova AV, Koch MHJ, Svergun DI (2003) PRIMUS: AWindows PC-based system for small-angle scattering data analysis. *J Appl Cryst* 36: 1277–1282.
18. Fisher H, de Oliveira Neto M, Napolitano HB, Polikarpov IL, Craievich AF (2010) Determination of the molecular weight of proteins in solution from a single small-angle X-ray scattering measurement on a relative scale. *J Appl Cryst* 43: 101–109.
19. Svergun D, Barberato C, Koch MHJ (1995) CRYSOL - a program to evaluate X-ray solution scattering of biological macromolecules from atomic coordinates. *J Appl Cryst* 28:768–773.
20. Svergun DI, Petoukhov MV, Koch MH (2001) Determination of domain structure of proteins from X-ray solution scattering. *Biophys J* 80:2946–2953.
21. Volkov VV, Svergun DI (2003) Uniqueness of *ab initio* shape determination in small-angle scattering. *J Appl Cryst* 36:860–864.
22. Kozin MB, Svergun DI (2001) Automated matching of high- and low-resolution structural models. *J Appl Cryst* 34:33–41.
23. Noirot-Gros MF, et al. (2006) Functional dissection of YabA, a negative regulator of DNA replication initiation in Bacillus subtilis. *Proc Natl Acad Sci USA* 103: 2368–2373.
24. Martin B, Prudhomme M, Alloing G, Granadel C, Claverys JP (2000) Cross-regulation of competence pheromone production and export in the early control of transformation in Streptococcus pneumoniae. *Mol Microbiol* 38:867–878.
25. Eckert K, et al. (2010) The Pih1-Tah1 cochaperone complex inhibits Hsp90 molecular chaperone ATPase activity. *J Biol Chem* 285:31304–31312.
26. Guiral S, et al. (2006) Construction and evaluation of a chromosomal expression platform (CEP) for ectopic, maltose-driven gene expression in Streptococcus pneumoniae. *Microbiology* 152:343–349.
27. Martin B, et al. (2010) Expression and maintenance of ComD-ComE, the two-component signal-transduction system that controls competence of Streptococcus pneumoniae. *Mol Microbiol* 75:1513–1528.
28. Zeghouf M, et al. (2004) Sequential Peptide Affinity (SPA) system for the identification of mammalian and bacterial protein complexes. *J Proteome Res* 3:463–468.
29. Lecointe F, et al. (2007) Anticipating chromosomal replication fork arrest: SSB targets repair DNA helicases to active forks. *EMBO J* 26:4239–4251.
30. Cormack BP, Valdivia RH, Falkow S (1996) FACS-optimized mutants of the green fluorescent protein (GFP). *Gene* 173(1 Spec No):33–38.
31. Lemon KP, Grossman AD (1998) Localization of bacterial DNA polymerase: Evidence for a factory model of replication. *Science* 282:1516–1519.
32. Sambrook J, Fritsch EF, Maniatis T (1989) *Molecular Cloning. A Laboratory Manual* (Cold Spring Harbor Laboratory, Cold Spring Harbor, NY), 2nd Ed.

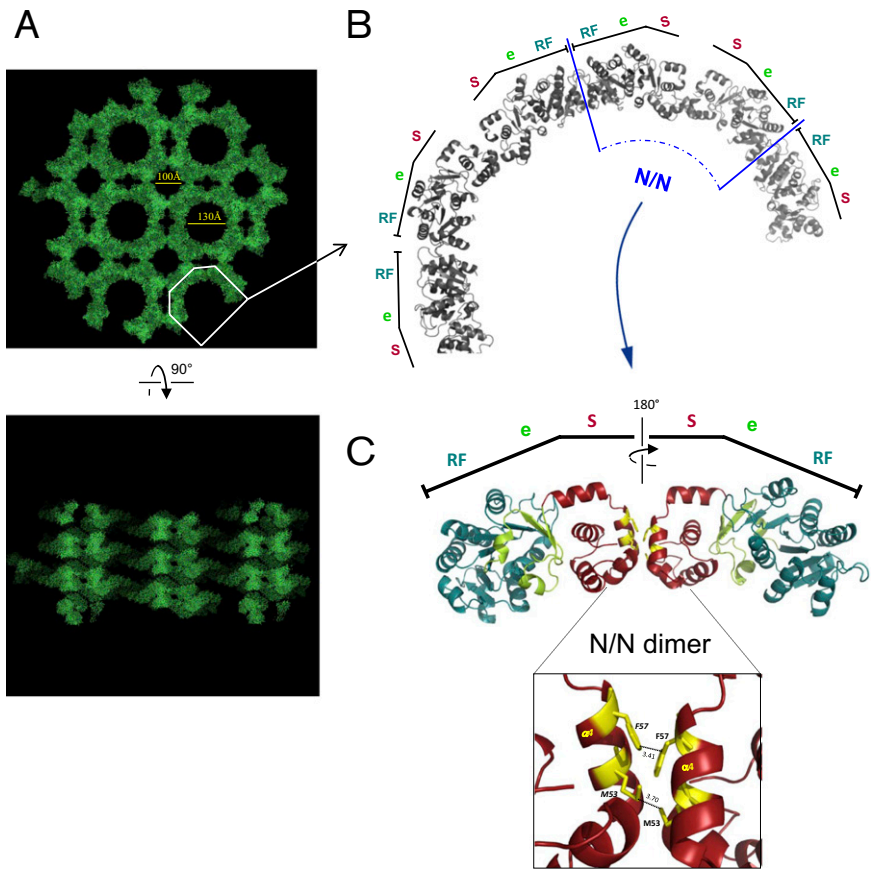

Fig. S1. DprA dimers in the crystal. (*A*) Crystal lattice of DprA showing large channels delineated by long polymers of C/C dimers connected via SAM domains. Filamentous packing of DprA in the crystal relies on both C/C (Fig. 1*D*) and N/N interactions (see panel *C*). (*B*) Enlarged view of a portion of the DprA polymer composed of three dimers. Dimers are represented as ribbon diagrams uniformly colored in gray (see Fig. 1*D* and panel *C* below for details). Comparison of the three monomers in the asymmetric unit indicates that the SAM (S) and extended Rossmann fold (eRF) are relatively fixed to one another in the crystal packing. They are nearly identical in the three DprA copies, exhibiting very low rmsd values (around 0.15 Å), although the two domains display some slight (1–2°) variability in their relative orientation. (*C*) Ribbon schematic presentation of an N/N DprA dimer. An angle of 100–120° is generated between N-terminal interfacing monomers. The N/N interaction involves the α4 of SAMs from two adjacent monomers; a small hydrophobic interaction surface (PISA server: 673 $Å^2$) with residues L36, L37, G38, P49, A50, V51, M53 seems mainly stabilized via packing of the aromatic rings of the two F57 residues. The color code is as in Fig. 1*A*. See legend of Fig. 1*D* for details.

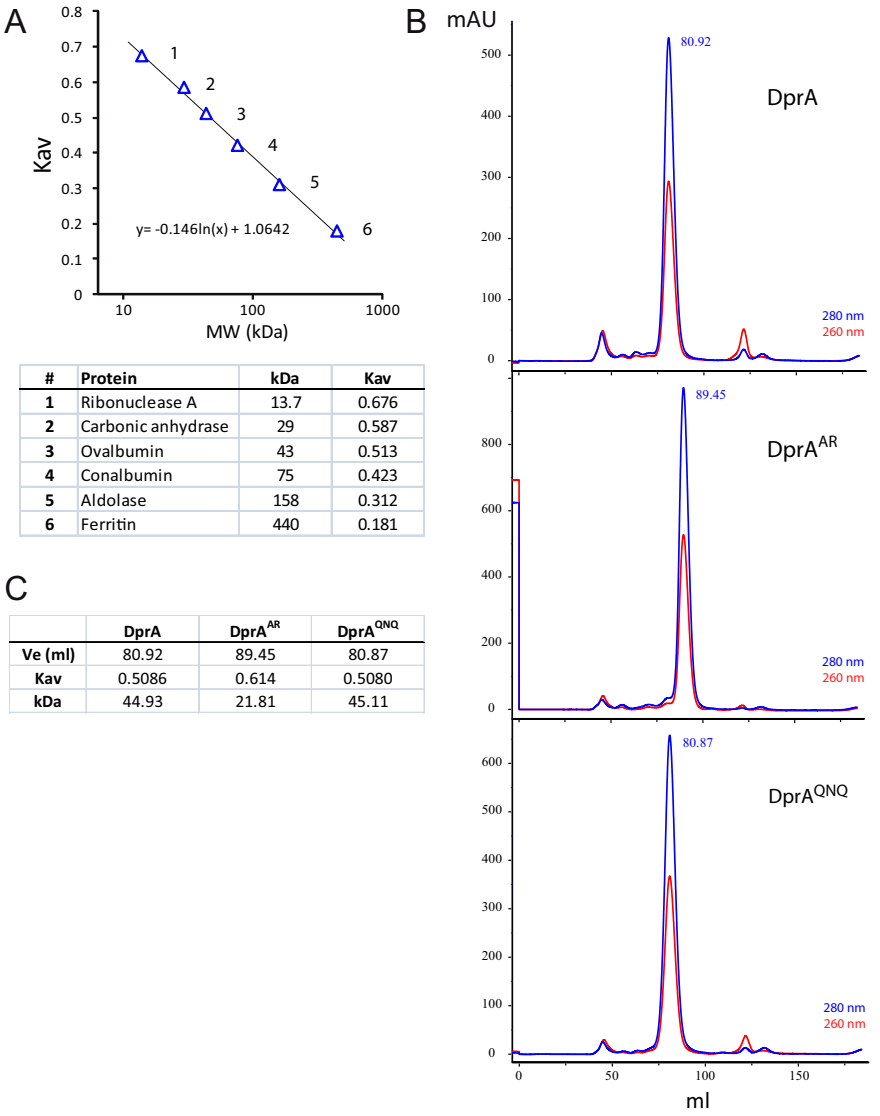

#	Protein	kDa	Kav
1	Ribonuclease A	13.7	0.676
2	Carbonic anhydrase	29	0.587
3	Ovalbumin	43	0.513
4	Conalbumin	75	0.423
5	Aldolase	158	0.312
6	Ferritin	440	0.181

C

	DprA	DprA^{AR}	DprA^{QNQ}
Ve (ml)	80.92	89.45	80.87
Kav	0.5086	0.614	0.5080
kDa	44.93	21.81	45.11

Fig. S2. Gel filtration analysis of DprA, DprA^{AR}, and DprA^{QNQ}. (*A*) Calibration of the Superdex 200 HL 16/60 column (GE Healthcare) using standard proteins (from GE Healthcare) with known molecular masses. The value of the partition coefficient K_{av} [K_{av} = (Ve − Vo)/(Vt − Vo), where Ve is the elution volume of the protein, Vo is the void volume, and Vt is the total volume] of each standard protein is plotted as a function of its molecular mass (MW). (*B*) Elution chromatograms of purified DprA, DprA^{AR}, and DprA^{QNQ}. Elution was run at 1 mL·min^{-1} at 4 °C and monitored at 280 nm (blue) and 260 nm (red) wavelengths. The column was equilibrated in the same buffer as the protein samples [50 mM MES (pH 6.5), 2 M NaCl, 5 mM β-mercaptoethanol]. (*C*) Calculated K_{av} of DprA, DprA^{AR}, and DprA^{QNQ} and an estimate of their apparent molecular masses.

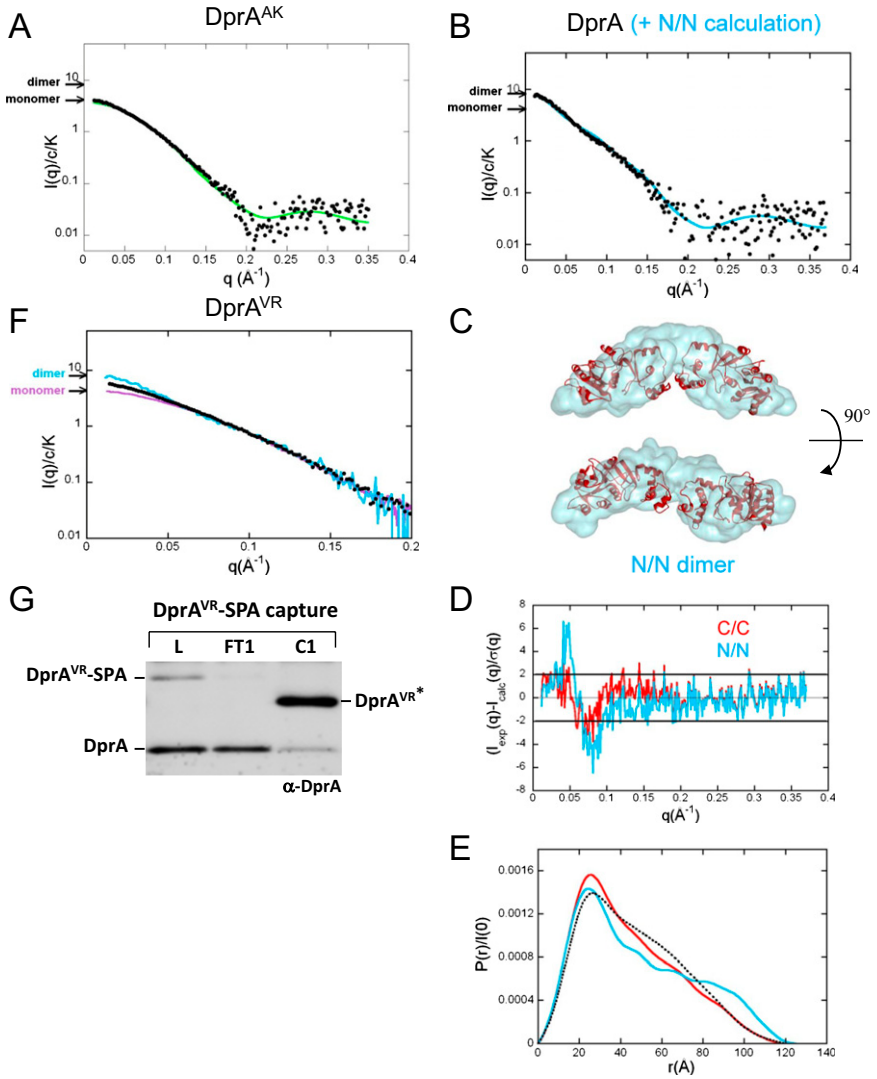

Fig. S3. *C*/*C*-dependent DprA dimerization in solution and oligomerization in pneumococcal cells. (*A*) SAXS analysis of purified DprA^{AK} mutant. Experimental scattering curve *I*(*q*) (black dots) of DprA^{AK} superimposed on the curve calculated from the crystal structure of the DprA monomer (green line). See *SI Materials and Methods* for details. (*B*) Adjustment of the curve calculated from the crystal structure of the N/N dimer to the experimental scattering curve of DprA. χ = 1.8, indicating a weaker fit for the N/N dimer than for the *C*/*C* dimer (Fig. 3*A*). (*C*) Crystal structure of the N/N dimer superimposed on a typical envelope of the protein deduced from the SAXS experimental curve using the program GASBOR. The lower envelope is rotated 90° on the horizontal axis compared with the top envelope. (*D*) Reduced residuals of the least-square fits: $I_{exp}(q) - I_{calc}(q)/\sigma_{exp}$, shown on a linear scale. Two horizontal lines define the ± 2 range. Red curve, *C*/*C* dimer; blue curve, N/N dimer. (*E*) Distance distribution functions *p*(*r*). Black dotted line, experimental curve; red curve, *C*/*C* dimer; blue curve, N/N dimer. The curve for the N/N dimer is rather distant from the experimental curve. The curve for the *C*/*C* dimer fits the experimental data better, but the remaining variations (shoulder of the experimental curve at 60 Å) suggests a deviation angle of 20–30° between the two monomers in solution compared with the dimer in the crystal. (*F*) Superimposition of the experimental scattering curve *I*(*q*) of the DprA^{VR} mutant (black dots) on the curve of the DprA dimer (light blue) and the curve of the DprA^{AR} monomer (purple). (*G*) Copurification of DprA and SPA-tagged DprA^{VR} from pneumococcal cells. Total extracts from *dprA*$^+$ competent cells ectopically expressing the DprA^{VR}-SPA fusion were immunoprecipitated and analyzed as described in the legend of Fig. 3*E*. Asterisk indicates tagged DprA^{VR} released by proteolysis.

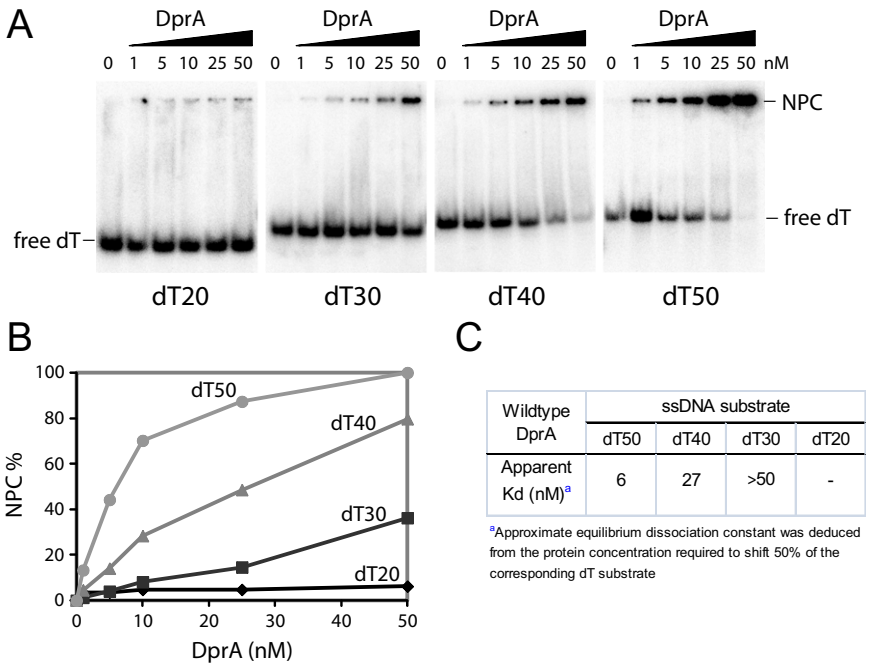

Wildtype DprA	ssDNA substrate			
	dT50	dT40	dT30	dT20
Apparent Kd (nM)[a]	6	27	>50	-

[a]Approximate equilibrium dissociation constant was deduced from the protein concentration required to shift 50% of the corresponding dT substrate

Fig. S4. Investigation of dT oligonucleotide size limit for nucleoprotein complex (NPC) detection by EMSA. (*A*) EMSA of DprA binding to ^{32}P-dT20 to ^{32}P-dT50 probes. See legend of Fig. 4*D* for details. (*B*) Quantification of EMSA experiments shown in *A*. (*C*) Calculated apparent K_d for the binding of DprA to dT20–dT50 oligonucleotides.

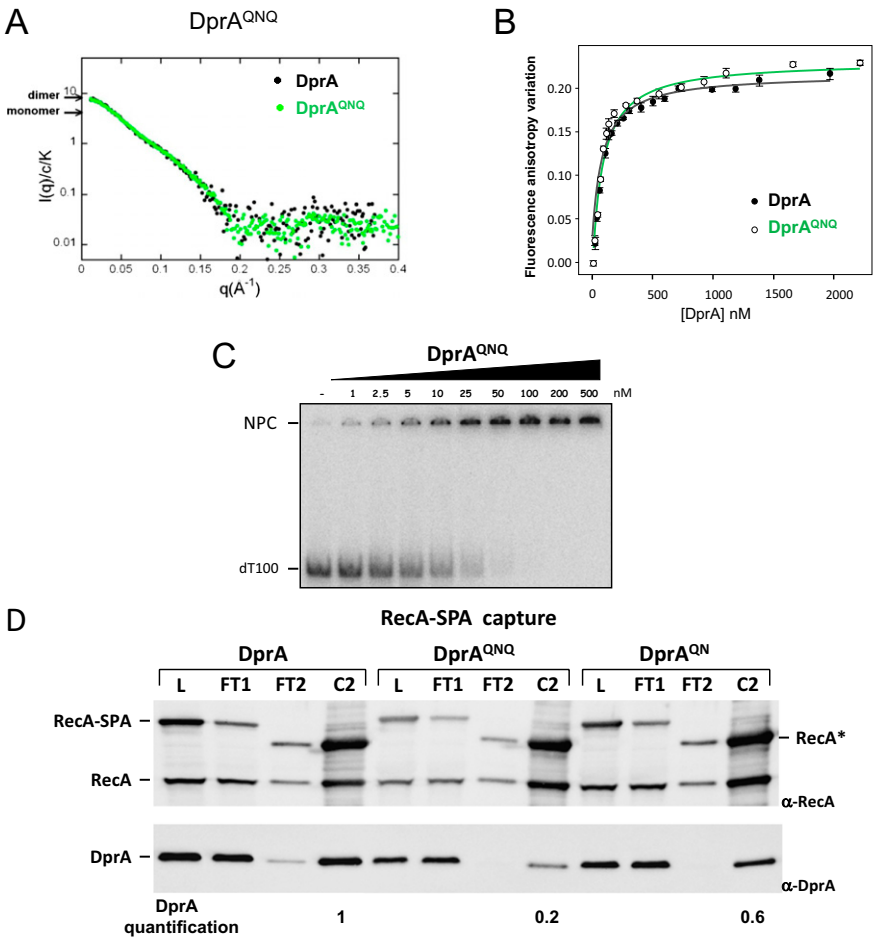

Fig. S5. In vitro and in vivo characterization of DprA^{QNQ} as a DprA–RecA interaction mutant. (*A*) SAXS analysis indicates that DprA^{QNQ} is a dimer in solution. Experimental scattering curve *I*(*q*) of DprA (black dots; taken from Fig. 3*A*) superimposed on the curve of DprA^{QNQ} (green dots). See legend of Fig. 3*A* for details. (*B*) Equilibrium binding of DprA and DprA^{QNQ} to fluorescein-labeled dT20. Anisotropy variation for DprA^{QNQ} (white circles) and DprA (black circles) fit a single-ligand–binding model (green curve for DprA^{QNQ}, K_d of 88 ± 6 nM; black curve for DprA, K_d of 75 ± 5 nM). (*C*) EMSA of DprA^{QNQ} binding to a ^{32}P-dT100 probe. See legend of Fig. 4*D* for details. Apparent K_d calculated for DprA^{QNQ}, 14 nM. (*D*) Cocaptures of DprA (*Left*), DprA^{QNQ} (*Center*), and DprA^{QN} (*Right*) using RecA-SPA expressed ectopically in *recA*$^+$ cells harboring the *dprA*$^+$, *dprA*^{QNQ}, or *dprA*^{QN} alleles. See legend of Fig. 5*A* for details.

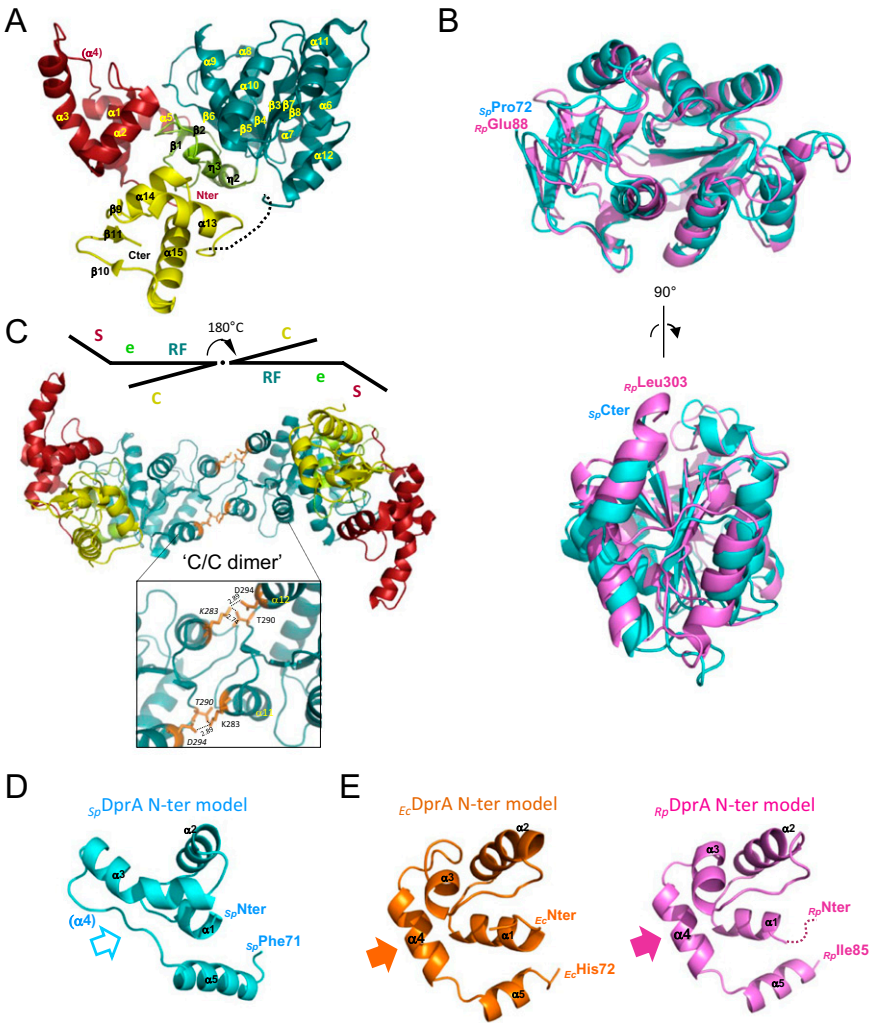

Fig. S6. Evolutionary conservation of DprA structural features. (*A*) Ribbon schematic presentation of the 3D structure of $_{Rp}$DprA. Color code is as in Fig. 1*A*; yellow, C-terminal extradomain of $_{Rp}$DprA. Dotted line denotes residues that were unresolved in the electron density map. (*B*) Superimposition of the eRF of $_{Sp}$DprA and $_{Rp}$DprA. Limits of eRF: $_{Sp}$DprA, residues 72–282; $_{Rp}$DprA, residues 88–303. Color code: cyan, $_{Sp}$DprA; purple, $_{Rp}$DprA. (*C*) Ribbon schematic presentation of the 3D structure of the $_{Rp}$DprA C/C dimer. See legend of Fig. 1*D* for details. (*D*) 3D modeling of $_{Sp}$DprA N-terminal based on $_{Rp}$DprA coordinates does not predict a SAM because α4, one of five helices characteristic of SAM, is missing (open arrow). (*E*) $_{Rp}$DprA and $_{Ec}$DprA N-terminal structures predicted by 3D modeling based on $_{Sp}$DprA coordinates. Both N-terminals folded as a bona fide SAM. Solid arrows indicate α4.

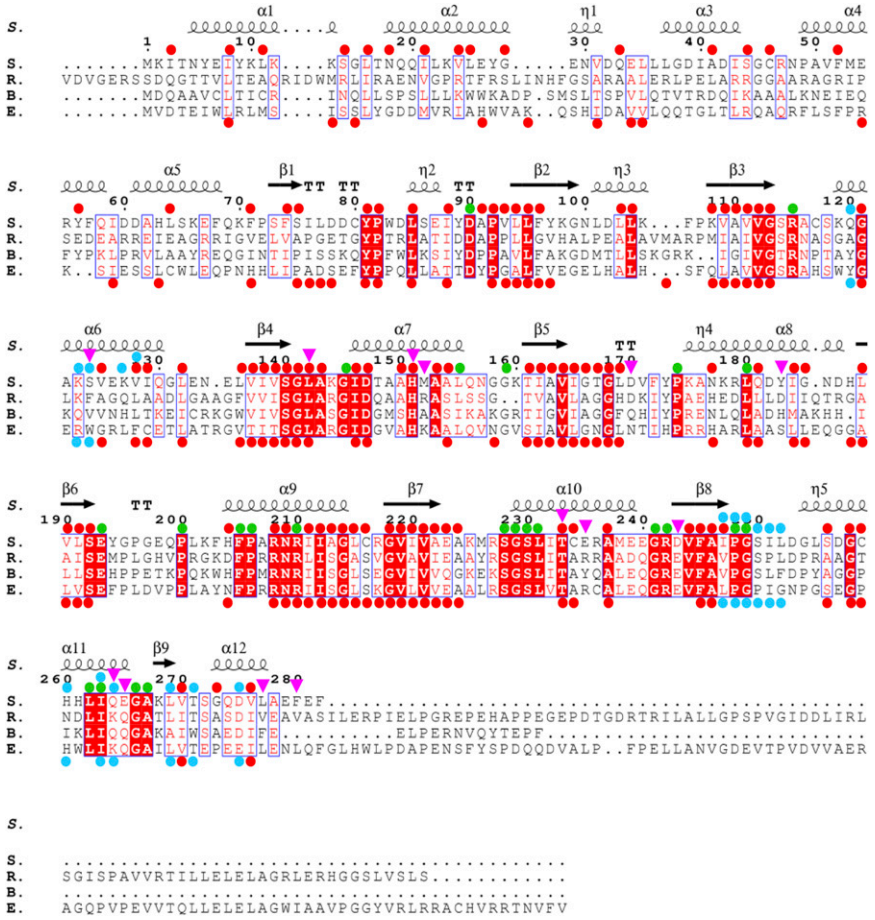

Fig. S7. Primary sequence alignment of $_{Sp}$DprA, $_{Rp}$DprA, $_{Bs}$DprA, and $_{Ec}$DprA. The multialignment was generated by Clustalw2 using Blosum weight matrix (1). The figure reflecting the homology degree (i.e., identical residues shown in white over a red background and boxing of conserved residues) was generated using ESPript 2.2 (2). $_{Sp}$DprA secondary structure elements (S) have been superposed on the sequences by ESPript 2.2. Symbols above and below alignments concern $_{Sp}$DprA and $_{Rp}$DprA, respectively. Red dots indicate buried residues; blue dots indicate dimerization interface residues based on structural data (Table S2); green dots indicate conserved surface residues; purple triangles indicate $_{Sp}$DprA mutants affecting interaction with RecA (Fig. 2*B*). B, *Bacillus subtilis*; E, *E. coli*; R, *Rhodopseudomonas palustris*; S, *S. pneumoniae*.

1. Larkin MA, et al. (2007) Clustal W and Clustal X version 2.0. *Bioinformatics* 23:2947–2948.
2. Gouet P, Courcelle E, Stuart DI, Métoz F (1999) ESPript: Analysis of multiple sequence alignments in PostScript. *Bioinformatics* 15:305–308.

Table S1. Diffraction data and refinement statistics

Diffraction data	SAD dataset*	Native dataset
Wavelength (Å)	0.9796	0.9330
Unit cell parameters (Å)	$a = b = 297.64$; c = 82.01	$a = b = 300.24$; c = 78.34
Space group	$I4_122$	
Resolution limits (Å)[†]	20.0–3.4 (3.5–3.4)	41.8–2.7 (2.8–2.7)
Number of observations measured[†]	214,469 (17,729)	241,160 (30,526)
Number of unique reflections measured[†]	47,748 (3,933)	474,506 (7,239)
Completeness (%)[†]	98.9 (98.3)	95.9 (92.4)
I/sI	11.6 (1.9)	11.6 (3.1)
Rmeas (%)[†,‡]	9.4 (75.7)	11.1 (46.4)
Refinement		
Number of nonhydrogen atoms (protein/water/other)	—	6542/165/25
Resolution range (Å)	—	41.8–2.7
R/R_{free} (%)	—	21.93/24.51
R.M.SD bonds (Å)/angles (°)	—	0.009 /1.13
Bfact($Å^2$) protein/water/other	—	58.6/47.8/76.8
Ramachandran plot (%) preferred/allowed/outliers	—	93.0/6.9/0.1

*Friedel mates were treated as separate reflections.

[†]Values in parentheses refer to the highest-resolution shell (2.8–2.7Å).

[‡]Rmeas = $\Sigma_h\Sigma_i |I_{h,i} - \langle I_h \rangle| / \Sigma_h \Sigma i\, I_{h,i}$, where $\langle I_h \rangle$ is the mean intensity for reflection h and $I_{h,i}$ is the i^{th} observation of reflection I_h.

Table S2. Accessibility of residues involved in dimerization of $_{Sp}$DprA and their conservation in $_{Rp}$DprA

$_{Sp}$DprA								$_{Rp}$DprA								
				Accessibility in								Accessibility in				
				Monomer		Dimer						Monomer		Dimer		
Residue	Location	Interacts with	Type	ASA	%	BSA	%	Residue	Location	Interacts with	Type	ASA	%	BSA	%	Other DprAs*
Q120	α6	L252	Hph	115.1	80	18.7	64	A139	α6	L271	Hph	80.5	100	13.9	80	YY
K123	α6	L252	Hph	136.1	81	20.3	65	**K142**	α6	L271	Hph	161.8	97	12.1	87	QR
S124	α6	I251-L252	Hph	34.8	43	25.5	9	F143	α6	P270-L271	Hph	55.1	31	20.3	19	VW
K127	α6	I251-L252	Hph	120.6	72	39.1	43									QHL†
V128	α6	I251	Hph	3.4	3	2.8	0									LLF†
I247	β8	I251	Hph	13.7	10	9.4	3	V266	β8	P270	Hph	20.1	24	11.0	10	VL
P248		G249-H260	Hph	49.8	47	43.8	5	**P267**		G268-P270	Hph	47.7	45	42.7	5	++
G249		P248-S250	Hph	38.4	100	28.2	20	**G268**		P267-S269	Hph	30.9	100	26.7	10	++
S250		G249	Hph	46.8	59	20.6	30	**S269**		G268	Hph	60.9	100	18.0	70	+P
I251		S124-K127-V128 -I247-T271	Hph	147.7	100	139.2	0	P270		F143-P267-T290	Hph	126.0	100	88.0	30	L+
L252		Q120-K123 -S124-K127	Hph	164.3	100	106.5	30	**L271**		A139-K142-F143	Hph	163.3	100	29.8	80	FG
H260	α11	P248-T271	Hph	39.0	26	37.7	0	N279	α11	T290	Hph	34.9	31	31.4	0	I+
I263	α11	L269	Hph	42.6	30	27.3	9	**I282**	α11	L288	Hph	42.3	30	28.0	9	++
Q264	α11	L269-D275	Hyd	151.3	100	68.1	50	K283	α11	D294-T290	Sal+Hyd	160.4	100	89.7	40	+K
L269	β9	Q264-D275, I263	Hyd, Hph	78.2	57	74.4	0	**L288**	β9	I282-K283	Hph	84.8	62	78.4	0	A+
T271		H260-I251	Hph	79.4	78	50.7	23	**T290**		K283	Hyd	84.4	50	51.2	30	W+
D275	α12	Q264-L269	Hyd	39.3	37	13.5	22	**D294**	α12	K283	Sal+Hyd	45.1	43	22.8	17	+E

Bold type indicates the presence of identical residues in $_{Sp}$DprA and $_{Rp}$DprA. For a view of $_{Sp}$DprA and $_{Rp}$DprA dimerization interfaces see Fig. 1*D* and Fig. S6*C*, respectively. Type of interaction: Hph, hydrophobic; Hyd, hydrogen; Sal, salt bridge. Accessibility: ASA, accessible surface area (Å^2) in the monomer; BSA, buried surface area (Å^2), i.e., surface engaged in the dimerization interface; % accessibility was calculated as indicated in *SI Materials and Methods*.

*Residue in $_{Bs}$DprA and $_{Ec}$DprA, respectively; +, residue identical to that in $_{Sp}$DprA; for an alignment of these proteins with $_{Sp}$DprA, see Fig. S7.

†First residue, $_{Rp}$DprA.

Table S3. Evolutionary conservation of DprA residues involved in interaction with RecA

		$_{Sp}$DprA						
		Accessibility* in						
		Monomer		Dimer			Mutants of $_{Sp}$DprA[†]	
Residue	Location	ASA	%	BSA	%	Other DprAs[‡]	1	2
S124	α6	34.8	43	25.5	9	FVW		P (+152T)
L142		0	0	—	0	+++	P	
H151	α7	0	0	—	0	+++	R	
M152	α7	90.6	57	0	57	RAK		T (+124P)
D170		39.9	38	0	38	+QN		G (+233P)
Y183	α8	98.7	53	0	53	DHS		H (+277P)
T233	α10	4.8	5	—	5	+++		P (+170G)
E235	α10	63.5	46	0	46	RYR	G; Q	Q (+243N)
D243	β8	71.1	67	0	67	EEE	G; N	N (+235Q)
Q264	α11	151.3	100	68.1	50	K+K	R	
E265	α11	116.7	85	0	85	QQQ	G; Q	Q (+235Q+243N)
L277	α12	34.3	25	0	25	VF+		P (+183H)
F280		63.8	36	0	36	Na[§]	L	

The dark grey shading identifies residues for which accessibility is reduced in the dimer.

*Calculated as indicated in Table S2.

[†]1, single mutant; 2, double mutants, except for the DprA^{QNQ} triple mutant (gray shading).

[‡]Residue in $_{Rp}$DprA, $_{Bs}$DprA. and $_{Ec}$DprA, respectively; +, residue identical to that in $_{Sp}$DprA; for an alignment of these proteins with $_{Sp}$DprA, see Fig. S7.

[§]Not applicable; last residue in $_{Sp}$DprA not aligned because of the presence of a C-ter extradomain in $_{Rp}$DprA (Fig. S6*A*) and $_{Ec}$DprA, but note that the last residue in $_{Bs}$DprA is also an F.

Table S4. Pneumococcal strains and plasmids and primers used in this study

Strain	Description/Genotype	Source/reference
R304	R800 derivative, *nov1*, *rif23*, *str41*; Nov^R, Rif^R, Sm^R	(1)
R800	R6 derivative	(2)
R1501	R800 but Δ*comC*	(3)
R1818	R1501 but *hexA*Δ3::*ermAM*; Ery^R	(4)
R2184	R1818 but *dprA*$^{C234R-F245L}$; Ery^R	This study
R2185	R1818 but *dprA*^{E265G}; Ery^R	This study
R2186	R1818 but *dprA*^{D243G}; Ery^R	This study
R2187	R1818 but *dprA*$^{I251V-H260R}$; Ery^R	This study
R2188	R1818 but *dprA*^{E235G}; Ery^R	This study
R2189	R1818 but *dprA*$^{D257G-L269S}$; Ery^R	This study
R2190	R1818 but *dprA*^{Q264R}; Ery^R	This study
R2321	R1501 but CEP$_X$-*recA*-SPA (from plasmid pCN9); Kan^R	This study
R2585	R1501 but *dprA*$^{H260A-L269R}$ (from plasmid pKHS-*dprA*$^{H260A-L269R}$)	This study
R2607	R2585 but CEP$_X$-*recA*-SPA (from plasmid pCN9); Kan^R	This study
R2830	R1818 but *dprA*$^{E235Q-D243N-E265Q}$; Ery^R	This study
R2832	R1818 but *dprA*$^{E235Q-D243N}$; Ery^R	This study
R2963	R1501 but CEP$_X$-*dprA*-SPA (from plasmid pCN55); Kan^R	This study
R2964	R1501 but CEP$_X$-*dprA*$^{I251V-H260R}$-SPA (from plasmid pCN56); Kan^R	This study
R2966	R1501 but CEP$_X$-*dprA*$^{H260A-L269R}$-SPA (from plasmid pCN58); Kan^R	This study
R2973	R1818 but CEP$_X$-*recA*-SPA (from plasmid pCN9); Kan^R	This study
R2975	R2830 but CEP$_X$-*recA*-SPA; Kan^R	This study
R2976	R2832 but CEP$_X$-*recA*-SPA; Kan^R	This study
R3108	R2585 but *hexA*Δ3::*ermAM*; Ery^R	This study
Plasmids*		
pCEP	pSC101 derivative (i.e., low copy number plasmid) carrying CEP; Kan^R	(5)
pCEP$_X$	pCEP derivative containing the ComX-dependent promoter P$_X$ and the RBS of *ssbB*; Kan^R	(6)
pCN9	pCEP$_X$ derivative containing the *recA*-SPA construct; Kan^R	This study
pCN21	pCEP$_X$ derivative containing the *gfp$_{mut2}$*-SPA construct; Kan^R	This study
pCN55	pCEP$_X$ derivative containing the *dprA*-SPA construct; Kan^R	This study
pCN56	pCEP$_X$ derivative containing the *dprA*$^{I251V-H260R}$ -SPA construct; Kan^R	This study
pCN58	pCEP$_X$ derivative containing the *dprA*$^{H260A-L269R}$ -SPA construct; Kan^R	This study
pUC57	ColE1 derivative; Ap^R	Genscript USA
pUC57-*dprA*$^{E235Q-D243N-E265Q}$	pUC57 derivative carrying a 885-bp NcoI-XhoI synthetic fragment containing the *dprA*$^{E235Q-D243N-E265Q}$ -His fusion; Ap^R	Genscript USA
pET28- *dprA*$^{E235Q-D243N-E265Q}$	pET28 derivative expressing the DprA$^{E235Q-D243N-E265Q}$-His fusion; Kan^R	This study
pKHS	pET28 derivative; Kan^R	(7)
pKHS-*dprA*	pKHS derivative expressing the DprA-His fusion; Kan^R	This study
pKHS-*dprA*$^{I251-H260R}$	pKHS derivative expressing the DprA$^{I251V\ -H260R}$-His fusion; Kan^R	This study
pKHS-*dprA*$^{H260A-L269R}$	pKHS derivative expressing the DprA$^{H260A\ L269R}$-His fusion; Kan^R	This study

Ap, ampicillin; Ery, erythromycin; Kan, kanamycin; Nov, novobiocin; ^{R}, resistance; Rif, rifampicin; Sm, streptomycin.
*Plasmids replicating autonomously only in *E. coli*.

1. Mortier-Barrière I, de Saizieu A, Claverys JP, Martin B (1998) Competence-specific induction of *recA* is required for full recombination proficiency during transformation in Streptococcus pneumoniae. *Mol Microbiol* 27:159–170.
2. Lefèvre JC, Claverys JP, Sicard AM (1979) Donor deoxyribonucleic acid length and marker effect in pneumococcal transformation. *J Bacteriol* 138:80–86.
3. Dagkessamanskaia A, et al. (2004) Interconnection of competence, stress and CiaR regulons in Streptococcus pneumoniae: Competence triggers stationary phase autolysis of *ciaR* mutant cells. *Mol Microbiol* 51:1071–1086.
4. Caymaris S, et al. (2010) The global nutritional regulator CodY is an essential protein in the human pathogen *Streptococcus pneumoniae*. *Mol Microbiol* 78:344–360.
5. Guiral S, et al. (2006) Construction and evaluation of a chromosomal expression platform (CEP) for ectopic, maltose-driven gene expression in Streptococcus pneumoniae. *Microbiology* 152:343–349.
6. Martin B, et al. (2010) Expression and maintenance of ComD-ComE, the two-component signal-transduction system that controls competence of Streptococcus pneumoniae. *Mol Microbiol* 75:1513–1528.
7. Eckert K, et al. (2010) The Pih1-Tah1 cochaperone complex inhibits Hsp90 molecular chaperone ATPase activity. *J Biol Chem* 285:31304–31312.

Table S5. Primers used in this study

Primer	Sequence
SC*dprA*-1	TTTTCGGCCGATTAATTTAAGAAGGAGATATATATATGAAAATCACAAACTATGA
SC*dprA*-2	TTTTTGCGGCCGCAAATTCAAATTCCGCAAGAAC
SC*dprA*^{AR}-1	CAGACGGTTGCGCTCATTTGATTCAAGAAGGAGCAAAACGTGTCACCAGTGGGC
SC*dprA*^{AR}-2	GCCCACTGGTGACACGTTTTGCTCCTTCTTGAATCAAATGAGCGCAACCGTCTG
RecA8	AACCTCGAGTTCTTCAATTTCGATTTCAAGTTCATCG
RecA9	CGAATTCCATGGCGAAAAAACC
SPAtag1	TCTCTCGAGATGGAAAAGAGAAGATGGAA
SPAtag3	GCGGATCCTATAATCCGGCCGTCC
oCN21	GGCTCATGAGTAAAGGAGAAGAACTTTTCACTGGAG
oCN25	CCACTCGAGTCGGCCGGAACCTTTGTATAGTTCATCC
oCN26	GGCTCATGAAAATCACAAACTATGAAATC
DprA23	TCACTCGAGAAATTCAAATTCCGCAAGAACATC

Underlined letters indicate convenient restriction sites introduced into the primer.